NANO LETTERS

Letter

pubs.acs.org/NanoLett

Robust Large Gap Two-Dimensional Topological Insulators in Hydrogenated III−V Buckled Honeycombs

Christian P. Crisostomo,[†] Liang-Zi Yao,[†] Zhi-Quan Huang,[†] Chia-Hsiu Hsu,[†] Feng-Chuan Chuang,[*,†] Hsin Lin,[*,‡] Marvin A. Albao,[§] and Arun Bansil[∥]

[†]Department of Physics, National Sun Yat-Sen University, Kaohsiung 804, Taiwan

[‡]Centre for Advanced 2D Materials and Graphene Research Centre, National University of Singapore, Singapore 117546, Singapore

[¶]Department of Physics, National University of Singapore, Singapore 117542, Singapore

[§]Institute of Mathematical Sciences and Physics, University of The Philippines Los Baños, Los Baños 4031, Laguna, Philippines

[∥]Department of Physics, Northeastern University, Boston, Massachusetts 02115, United States

Supporting Information

ABSTRACT: A large gap two-dimensional (2D) topological insulator (TI), also known as a quantum spin Hall (QSH) insulator, is highly desirable for low-power-consuming electronic devices owing to its spin-polarized backscattering-free edge conducting channels. Although many freestanding films have been predicted to harbor the QSH phase, band topology of a film can be modified substantially when it is placed or grown on a substrate, making the materials realization of a 2D TI challenging. Here we report a first-principles study of possible QSH phases in 75 binary combinations of group III (B, Al, Ga, In, and Tl) and group V (N, P, As, Sb, and Bi) elements in the 2D buckled honeycomb structure, including hydrogenation on one or both sides of the films to simulate substrate effects. A total of six compounds (GaBi, InBi, TlBi, TlAs, TlSb, and TlN) are identified to be nontrivial in unhydrogenated case; whereas for hydrogenated case, only four (GaBi, InBi, TlBi, and TlSb) remains nontrivial. The band gap is found to be as large as 855 meV for the hydrogenated TlBi film, making this class of III−V materials suitable for room temperature applications. TlBi remains topologically nontrivial with a large band gap at various hydrogen coverages, indicating the robustness of its band topology against bonding effects of substrates.

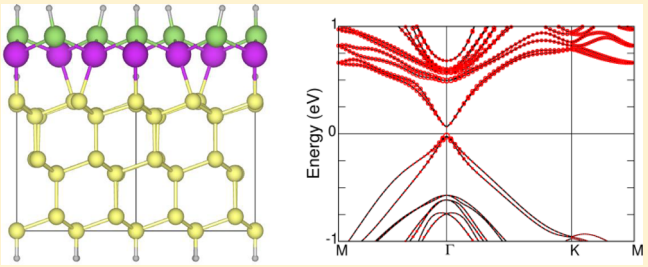

KEYWORDS: *2D topological insulators, topological phase transition, quantum spin Hall effect, III−V semiconductor thin films, electronic structures, first-principles calculations*

Topological insulators (TIs) have become one of the most widely studied materials in the past few years.[1,2] These novel materials are insulating in the bulk but support gapless edge states for two-dimensional (2D) TIs and gapless surface states for three-dimensional (3D) TIs, which are protected by powerful constraints of time-reversal symmetry. Although a number of 3D TIs have been synthesized experimentally, the 2D TIs, also known as quantum spin hall (QSH) insulators, are better suited for applications in spintronics and quantum computing in view of the remarkable robustness of their edge states against backscattering. The currently available QSH materials, however, are limited to quantum well systems[3−7] with very small band gaps observable only at very low temperatures (∼10 K). The search for 2D-TIs with large gaps thus presents an urgent challenge of great importance.

Inspired by the discovery of graphene,[8] a variety of atomically thin "beyond" graphene materials in the buckled honeycomb structure have been predicted to harbor the QSH phase. These include single layer Si (silicene), Ge (germanene),[9,10] Sn (stanene),[11] Bi,[12−14] strained As,[15] and Sb,[16,17] among others. However, a 2D thin film must eventually be grown or placed on a suitable substrate. But interactions with the substrate can modify the electronic structure of the film, which adds to the challenges of experimental realization of the QSH phase. A viable 2D film must not only display a nontrivial band topology but its electronic structure should also be insensitive to the effects of bonding with the substrate. Hydrogenation and the associated bonding may be viewed as a simplified model for simulating effects of the environment on the electronic structure of a film, including those of the substrate.[21−25] A number of studies indeed show that band topologies and band gaps in films are modified significantly upon hydrogenation[18−27] and that the structural changes induced by different functional groups can be modeled through effects of strain.[21,22]

A recent computational study[28] showed the dynamic stability of binary composition of group III−V in 2D buckled honeycomb structure and suggested possible synthesis and potential applications. We have previously predicted[29] un-

Received: June 9, 2015
Revised: September 2, 2015

DOI: 10.1021/acs.nanolett.5b02293
Nano Lett. XXXX, XXX, XXX−XXX

strained TlBi, GaBi, and InBi films to harbor the 2D TI phase. However, the key effects of the substrate have not yet been explored in III−V films. Here, we address this important issue by invoking a simplified electron-filling model for simulating effects of substrates on III−V thin films.

In order to identify new and robust QSH phases with large band gaps, we have carried out a first-principles study of 25 possible binary combinations of group III (B, Al, Ga, In, and Tl) and group V (N, P, As, Sb, and Bi) elements in the buckled honeycomb structure. We also consider effects of hydrogenation on one or both sides of each of these films, yielding a total of 75 films that were investigated. We predict QSH phases in both pristine and hydrogenated GaBi, InBi, TlBi, and TlSb, while TlAs and TlN exhibit a nontrivial phase only when the film is not hydrogenated. These films support a single Dirac cone edge state band for armchair edges with the Dirac point located in the middle of the 2D bulk gap, which is highly desirable for spin-transport applications.[30−32] This class of materials and their derivatives would also provide novel platforms for other applications more generally.[28,33,34]

Remarkably, we find an energy gap as large as 773 meV (or 855 meV) in TlBi films hydrogenated on one (or both) side. Moreover, by using TlBi as an exemplar system, we demonstrate that III−V films remain topologically nontrivial with a large band gap for various hydrogenation levels. Our analysis reveals why the electronic structure of TlBi is insensitive to hydrogenation, giving insight into how TlBi would provide an especially promising 2D TI, robust against deterioration via bonding effects of substrates.

Our first-principles computations have been carried out using the Vienna Ab-Initio Simulation Package (VASP).[35] Spin−orbit coupling (SOC) is included in the self-consistency cycles and band computations throughout this work unless indicated otherwise. Side views of the films hydrogenated on one or both sides, along with the associated Brillouin zones, are shown in Figure 1. One monolayer (ML) coverage corresponds to the number of hydrogens being equal to the number of III−V atoms in the unit cell. For two-sided hydrogenation, hydrogen atoms are adsorbed on opposite sides of the honeycomb with respect to the neighboring H atom, while for one-sided hydrogenation, all hydrogens are adsorbed on the same side of the honeycomb. Atomic positions were optimized without SOC for each lattice constant considered. Band structures and band topologies including spin−orbit coupling effects were computed for various equilibrium geometries. A total number of 75 films considered in this study are obtained from 25 III−V binary combinations in three different configurations: pristine buckled honeycombs, and buckled honeycombs hydrogenated on one or both sides. In order to ascertain band topologies, we used the method of ref 36 for computing the Z_2 invariant in terms of the so-called *n*-field configuration of the system. We have previously used this method to determine the Z_2 invariant of silicene on Bi/Si(111) substrate.[37] Since III−V films do not possess a center of inversion symmetry, parity analysis cannot be applied.[38] All topological phases were further checked by considering the evolution of band structures as a function of the strength of the SOC by adding a weighting factor WSOC (weighted SOC) to scale the SOC contribution in the computations.[16]

In this way, we identify six films (GaBi, InBi, TlBi, TlAs, TlSb, and TlN) as being nontrivial in the unhydrogenated case. TlAs and TlN are in the trivial phase when hydrogenated on one or both sides, while the other four films remain nontrivial after hydrogenation. Tables 1 and 2 give structural details and values of various gaps for the six films with and without hydrogenation. Similar details for all 75 films investigated are given in the Supporting Information in the interest of brevity. Notably, the present III−V buckled honeycombs remain buckled when hydrogenated (one side), unlike bismuth/antimony films which assume a planar structure upon hydrogenation,[23] although two-sided hydrogenation of Bi and Sb films also leads to a nearly planar structure.[23−25] For the

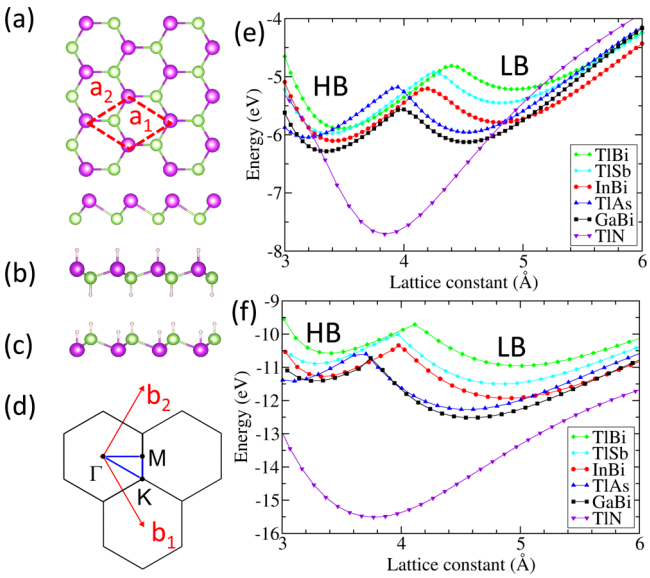

Figure 1. (a) Top and side views of the buckled honeycomb structure. (b and c) Side views of the two-sided (b) and one-sided (c) hydrogenated films. (d) 2D Brillouin-zones with specific symmetry points labeled. (e and f) Total energy as a function of the lattice constant for (e) pristine and (f) the two-side hydrogenated buckled honeycombs.

Table 1. Calculated Equilibrium Lattice Parameters, Band Gaps, and Topological Invariants (Z_2) for Selected Buckled Honeycombs without Hydrogenation

material	lat. const. (Å)	layer dist. (Å)	sys. gap (eV)	gap at Γ (eV)	gap at K (eV)	Z_2
GaBi	4.521	0.790	0.168	0.187	1.069	nontrivial
InBi	4.805	0.850	0.169	0.190	1.068	nontrivial
TlN	3.839	0.335	−0.061	0.083	2.842	nontrivial
TlAs	4.525	0.731	0.111	0.111	1.420	nontrivial
TlSb	4.815	0.806	0.274	0.274	1.025	nontrivial
TlBi	4.928	0.850	0.560	0.704	0.726	nontrivial

Table 2. Calculated Equilibrium Lattice Parameters, Band Gaps, and Topological Invariants (Z_2) for Selected Buckled Honeycombs with Hydrogenation on Both Sides

material	lat. const. (Å)	layer dist. (Å)	sys. gap (eV)	gap at Γ (eV)	gap at K (eV)	Z_2
GaBi	4.544	0.820	0.169	0.169	5.084	nontrivial
InBi	4.828	0.886	0.190	0.190	4.594	nontrivial
TlN	3.768	0.842	1.007	1.007	5.635	trivial
TlAs	4.505	0.897	0.233	0.233	5.013	trivial
TlSb	4.773	0.934	0.063	0.063	4.669	nontrivial
TlBi	4.914	0.913	0.855	1.050	3.964	nontrivial

DOI: 10.1021/acs.nanolett.5b02293
Nano Lett. XXXX, XXX, XXX−XXX

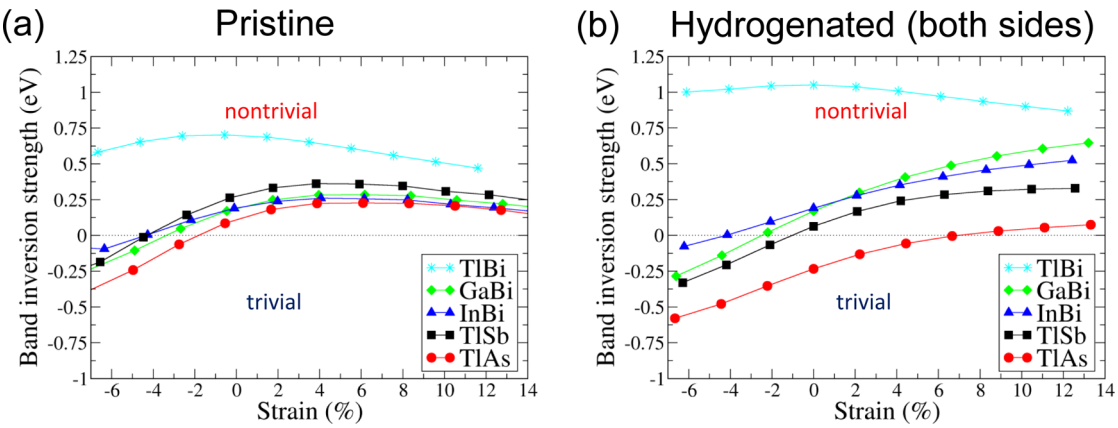

Figure 2. Band inversion strength (BIS) as a function of strain for (a) pristine and (b) hydrogenated (both sides) buckled honeycombs. Buckled honeycombs with positive and negative BIS values are in the topological insulator and normal insulator phase, respectively.

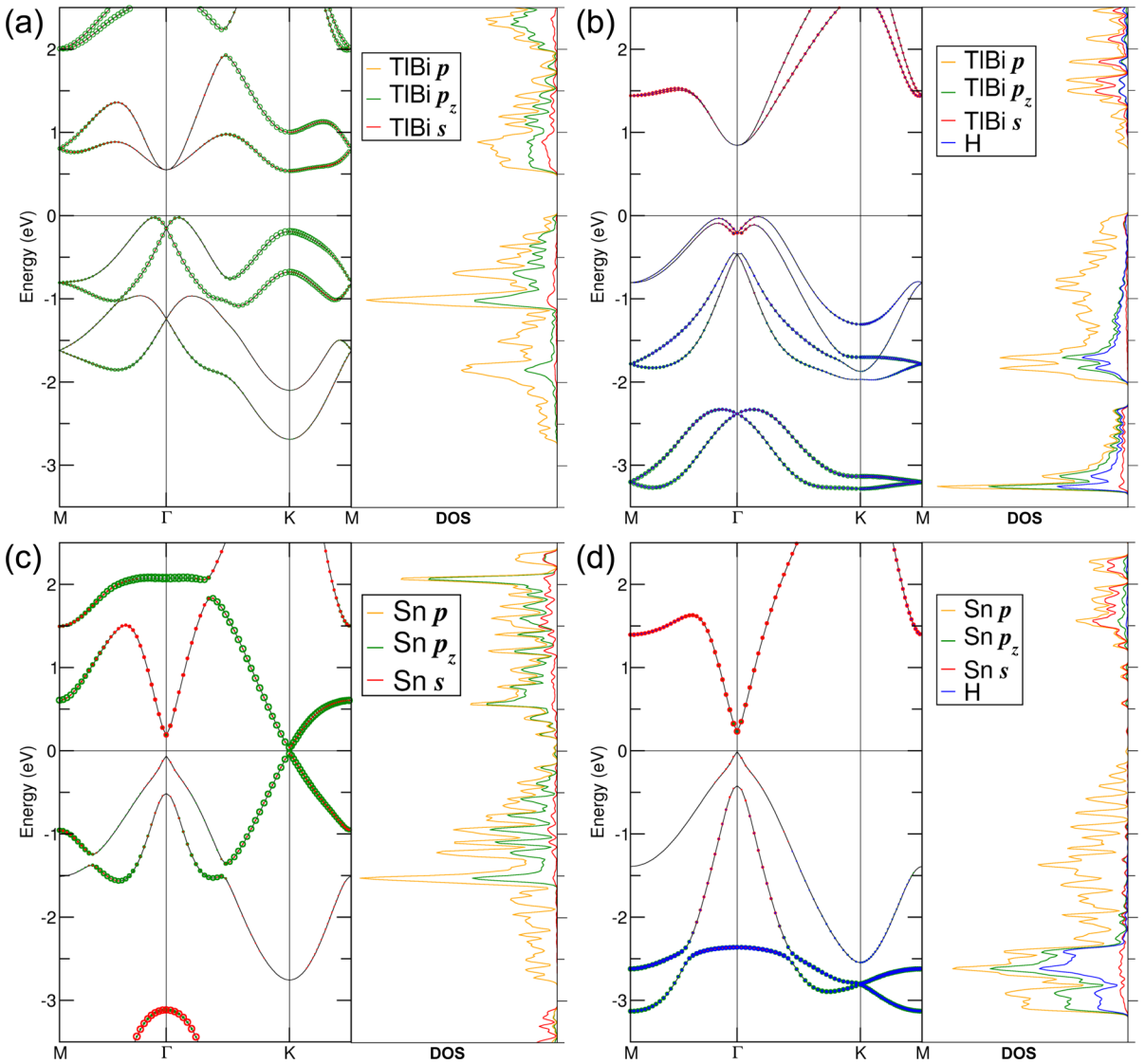

Figure 3. Band structures and partial densities of states (DOSs) associated with various orbitals in TlBi and Sn films: (a) unhydrogenated bilayer of TlBi; (b) hydrogenated (both sides) buckled honeycomb of TlBi; (c) unhydrogenated buckled honeycomb of Sn; and, (d) hydrogenated (both sides) buckled honeycomb of Sn. Sizes of dots of various colors are proportional to the partial DOSs from different orbitals as follows: red dots for s-orbital from Tl and Bi (Sn in c and d); green dots for p_z-orbital; and blue dots for the H s-orbital. For the partial DOSs, solid lines of various colors give contributions from different orbitals as indicated in the legends in a–d.

DOI: 10.1021/acs.nanolett.5b02293
Nano Lett. XXXX, XXX, XXX−XXX

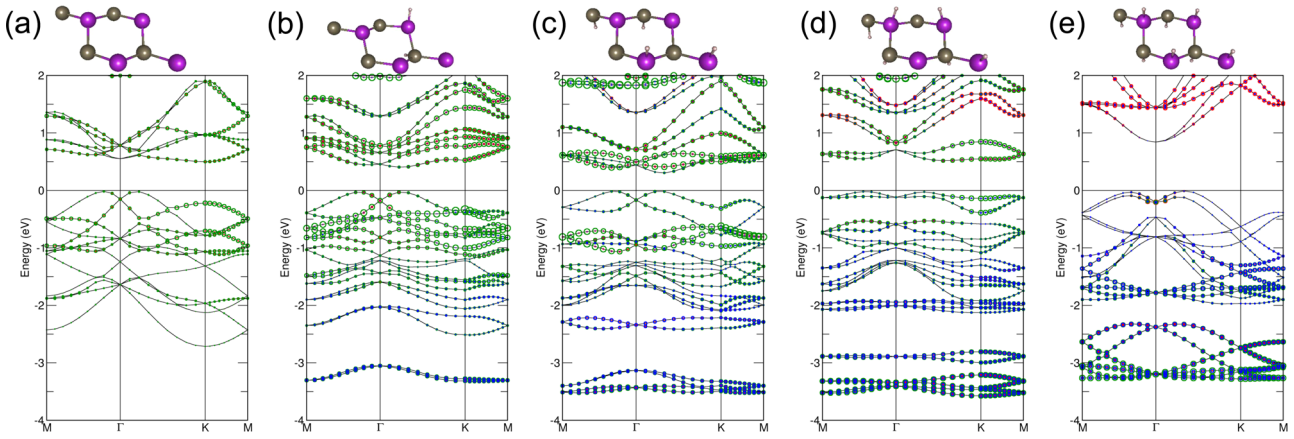

Figure 4. Band structures for (a) 0, (b) 0.25, (c) 0.50, (d) 0.75, and (e) 1 ML hydrogen coverages. The lowest energy structure used in the computations is shown on the top of each panel. Sizes of red, green, and blue dots are proportional to the contributions of s- and p_z-orbitals of Tl and Bi and the s-orbital of H, respectively.

remainder of our discussion, we will focus on the unhydrogenated films and films hydrogenated on both sides.

Figure 1e gives the total energy per unit cell of the six aforementioned nontrivial films as a function of lattice constant *a*. The corresponding results for the hydrogenated (both sides) films are given in Figure 1f. Except for TlN, all films display two local minima in energy. We will refer to the corresponding stable phases as high-buckled (HB) and low-buckled (LB) states in order to highlight the size of buckling or interlayer distance in these two distinct states. With reference to Tables 1 and 2, the calculated equilibrium lattice constants in LB phase for GaBi, InBi, TlBi, TlAs, TlSb, and TlN are 4.521, 4.805, 4.928, 4.525, 4.815, and 3.839 Å for the pristine buckled honeycombs and 4.544, 4.828, 4.914, 4.505, 4.773, and 3.768 Å for the hydrogenated (both sides) buckled honeycombs, respectively. In general, the vertical interlayer distance in pristine films varies over 0.335−0.850 Å. The interlayer separation in the hydrogenated films is larger and varies over 0.820−0.934 Å. The band gaps are generally enhanced with hydrogenation of films with the exception of TlSb. The largest band gap of 855 meV is seen in the hydrogenated TlBi film.

We have examined the topological nature of all investigated films as a function of strain as shown in Figure 2. The QSH phase survives in five films (GaBi, InBi, TlBi, TlAs, and TlSb) over a wide range of strains. The pristine TlN film is a nontrivial semimetal, but a compressive strain of about −3% induces the TI phase. As for TlAs, it can be driven into the nontrivial topological phase through a strain larger than −2% and 6.7% for pristine and hydrogenated films, respectively. The band inversion strength (BIS), which we define as the direct band gap at Γ, provides a measure of how far the material is from a topological critical point. BIS is positive when the band is inverted (nontrivial) and negative (trivial) otherwise. Figure 2 gives BIS values as a function of strain for selected pristine and hydrogenated (both sides) buckled honeycombs.

We now discuss, with the representative examples of Sn, Bi, and TlBi, how hydrogenation modifies band topologies of films and how the effects of hydrogenation differ among group IV, group V, and III−V films. Hydrogenation in Sn causes the lattice constant to change by about 0.8%, from 4.68 to 4.72 Å,[21−23] and changes the band topology from being nontrivial to trivial. On the other hand, hydrogenation in Bi and Sb not only significantly changes the band structure but also results in structural transformation from a buckled to a planar honeycomb.[23,25] In sharp contrast, hydrogenation (two-sided) of TlBi films only induces a small strain (∼0.3%) without any significant distortion in the structure. This is a desirable characteristic of the III−V buckled honeycombs in that the lattice constants are essentially maintained upon hydrogenation.

Figure 3 highlights changes in band structures and partial densities of states (projected on various sites) when pristine films of TlBi and Sn are hydrogenated, these being the two exemplar cases in which hydrogenation causes a relatively small change in the lattice constant. Since the Sn buckled honeycomb possesses inversion symmetry, bands in Figure 3c and d are degenerate. When this symmetry is broken in the TlBi buckled honeycomb, the resulting bands in Figure 3a and b are different in general and show Rashba type splittings. Figure 3b and d show that the contribution of the H s-orbital, given by the size of blue dots, is mainly located around 3 eV below the Fermi energy. As for band inversion, we found that in TlBi it is a p−p type band inversion which takes place at Γ. Without the SOC, p_y-orbital of Bi lies above its p_x-orbital, but when the SOC is turned on, the order of these p_x and p_y orbitals is reversed. In fact, the H s-orbital is strongly hybridized with the p_z-orbital (green dots) of Tl and Bi, while it is only weakly hybridized with the s-orbital (red dots) of Tl and Bi. Hybridization with H atoms thus shifts unsaturated p_z orbitals from above to below the Fermi energy, so that the low binding energy states near the Fermi level now become dominated by other p- and s-orbitals. As a result, the band topology in TlBi remains nontrivial upon hydrogenation, while it becomes trivial in Sn. The band topology of Sn can however be further controlled via strain.[23]

Since hydrogenation does not alter the band topology of III−V films, we tested the robustness of the nontrivial phase by considering different levels of hydrogen coverage in TlBi films. Here, we define one monolayer (ML) coverage to correspond to two hydrogen atoms per TlBi pair. An augmented 2 × 2 supercell was used to simulate coverages of 1, 0.75, 0.5, 0.25, and 0 ML by removing/adding up to two hydrogen atoms in the supercell. Since there are several possible ways of removing or adding two hydrogens which lead to different total energies per supercell, we followed the scheme of a previous study[39] in which having the two H atoms on opposite sides of the neighboring C atoms in graphene yielded greater stability. As already noted, the lattice constants of pristine and fully hydrogenated films only differ by 0.3%. Therefore, we used the lattice constant of fully hydrogenated film for partial

DOI: 10.1021/acs.nanolett.5b02293
Nano Lett. XXXX, XXX, XXX−XXX

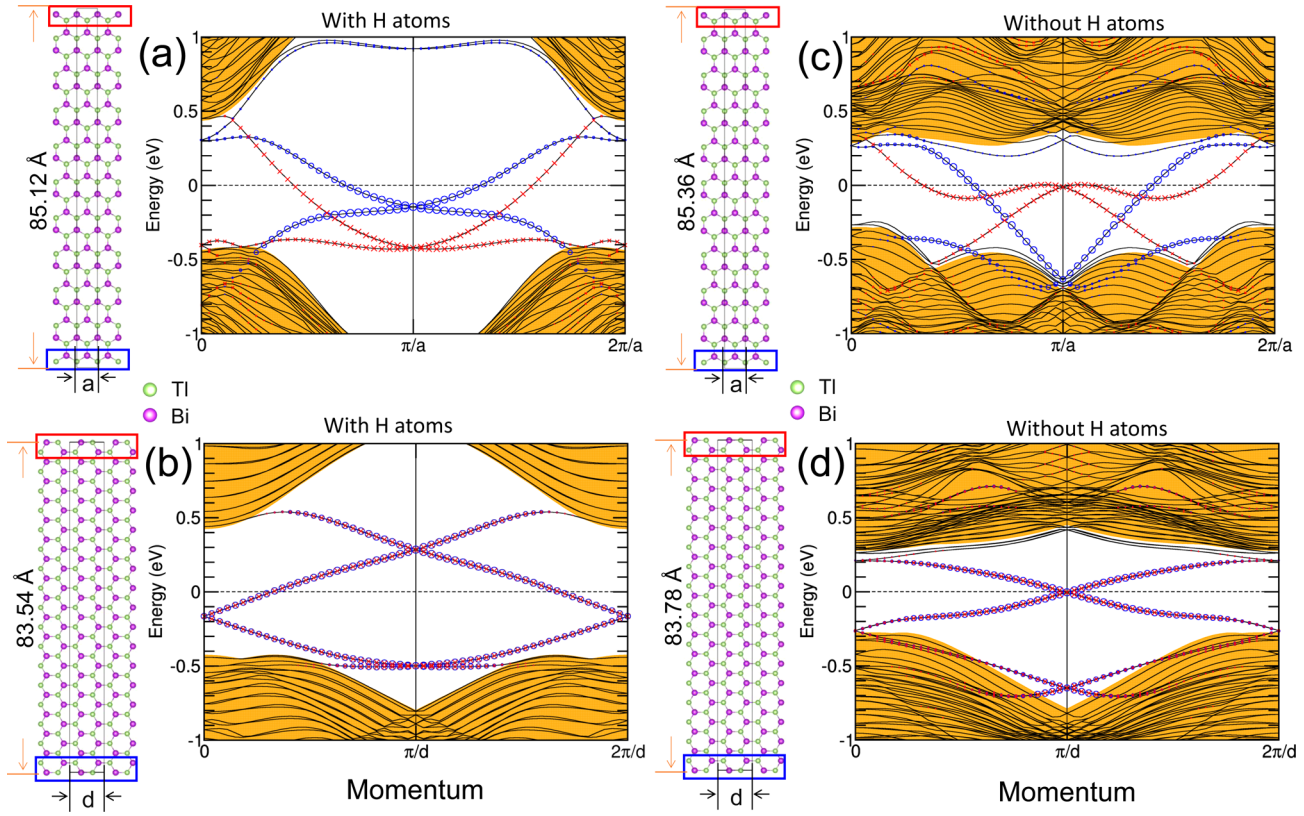

Figure 5. Crystal and band structures of hydrogenated (both sides) TlBi ribbons for (a) zigzag and (b) armchair edges. (c and d) Corresponding results for the pristine TlBi ribbons. Contribution from the top (bottom) edge is marked with red crosses (blue circles). Sizes of red crosses and blue circles are proportional to contributions from the respective edges. Region with orange filling denotes bulk bands. The zero energy is chosen to lie in the middle of the 2D bulk band gap.

coverages, while allowing the atoms to relax. Figure 4 shows the relaxed atomic structures with lowest energy at each coverage and the associated band structures for 0−1 ML coverages. Similar to Figure 3, the H contribution is seen to be mostly concentrated at low energies, and H s-orbital is partially hybridized with the p_z-orbital of Tl and Bi. The Z_2 invariant for all coverages remains nontrivial, and the unsaturated p_z-orbitals are pulled below the Fermi level. These results demonstrate that the topology of TlBi films is highly robust against chemical bonding effects of the environment, making these films particularly flexible with regard to substrate choices for potential device applications.

In order to assess the robustness of our calculations to the underestimation of band gap within the GGA, we computed the electronic and topological properties of all hydrogenated as well as unhydrogenated films in Tables 1 and 2 using the hybrid functional HSE06.[40] Under HSE06, among the unhydrogenated films, GaBi and TlAs assume the trivial phase, while for the hydrogenated films, only TlBi remains in the nontrivial phase. However, we find that (using HSE06), the unhydrogenated films under 3% and the hydrogenated films under 5% strain, essentially revert back to the GGA-based results in all cases. Our GGA-based results in Figure 2 thus correctly capture evolution of the topological phases with strain, some differences in the exact values of the strain at which phase transitions occur depending on the particular exchange-correlation functional employed in the computations notwithstanding.

Figure 5 compares the edge state spectrum in pristine and hydrogenated TlBi ribbons and gives insight into effects of hydrogenation on edge states. Widths of the ribbons were taken to be fairly large to reduce interaction between the two edges. Both armchair and zigzag edges were considered. The odd number of edge states crossing the Fermi level between 0 and π/a (π/d for armchair edge) confirms the Z_2 nontrivial phase of the system. The edge states in Figure 5 (red crosses and blue circles) are seen to be gapless with Dirac nodes at 0 or π/a, and span the bulk energy gap connecting the valence and conduction bands. The asymmetric termination of a zigzag ribbon provides two different dispersions of edge band where the bottom edge (blue circles) is Tl-terminated, while the top edge is Bi-terminated (red crosses). In contrast, in the armchair ribbon, both edges possess the same structure, and indeed the band structures for the two edges are the same as seen in Figure 5b and d. As the band gap increases with hydrogenation, the edge states mainly lie within the gap. The edge state spectrum in the pristine cases in panels c and d contains a single Dirac cone with its node lying in the middle of the 2D band gap for both zigzag and armchair ribbons. In the hydrogenated case, on the other hand, the nodes of the Dirac cones are seen to lie below and above the Fermi level for zigzag and armchair ribbons, respectively.

Finally, in order to gain insight into the viability of our simplified hydrogenation model for simulating substrate effects, we searched for a suitable substrate for supporting nontrivial phase of III−V films. Among various substrates such as Ge, Si, and SiC, we found that Si(111) would be a good candidate for supporting III−V films. In particular, $\sqrt{3} \times \sqrt{3}$ hydrogenated GaBi has a lattice constant of 7.87 Å, which is close to the lattice constant of 7.73 Å of 2×2 Si(111), so that this substrate could support a GaBi film (with small strain) and preserve its

DOI: 10.1021/acs.nanolett.5b02293
Nano Lett. XXXX, XXX, XXX−XXX

nontrivial phase (see Figure 2). With this in mind, we considered a GaBi film on Si(111) by using three Si(111) bilayers to simulate the substrate. The Si atoms in the bottom layer were passivated with H atoms and kept fixed. The top layer (either Ga or Bi) was also passivated with H, but all atoms in this case (including H) were allowed to relax. We also considered two possible types of bonding in which the top Si(111) layer can either bond with Ga or Bi atoms. Figure 6

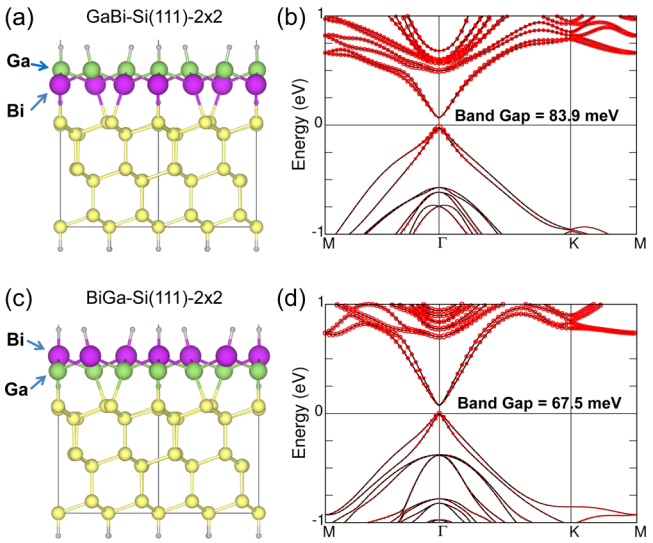

Figure 6. The relaxed structures of (a) GaBi and (c) BiGa on top of Si(111). The total s-orbital contribution (proportional to the size of red circles) of (b) GaBi and (d) BiGa are shown to have an inverted band at Γ, thus exhibiting nontrivial topological phase.

presents the crystal and band structures for these two different cases where the Ga layer lies on the top or below the Bi layer. The corresponding total *s-orbital* contributions to band structures when Ga lies on the top [GaBi-Si(111)-2 × 2] or below [BiGa-Si(111)-2 × 2] Bi with band gaps of 83.9 and 67.5 meV are also shown. The Z_2 parameter was calculated in both cases and found to correspond to the nontrivial phase with a gap that exceeds room-temperature thermal energy. Note that the band gap of the GaBi film is reduced (from 169 to 83.9 or 67.5 meV) when it is placed on the Si(111) substrate. This reduction, however, is driven by the smaller (theoretical) band gap of Si in our computations and reflects band realignment effects when the film is placed on the substrate. These results indicate the importance of size of the gap of the substrate as an important factor for maintaining the gap characteristics of a freestanding film and point to large-gap insulators as being generally more viable in this regard. Our study shows that hydrogenation would provide an efficient search tool for screening films for their viability in the presence of substrate effects, although actual computations will be needed for delineating the complexity of substrate effects in promising cases.

Through a study of 75 III−V buckled honeycombs without and with hydrogenation on one or both sides, we predict that unhydrogenated as well as hydrogenated GaBi, InBi, TlBi, TlSb films, in addition to the pristine and strained hydrogenated TlAs and TlN films, harbor the QSH phase with band gaps large enough for room-temperature applications. The hydrogenated (both sides) TlBi film supports an especially large band gap of 855 meV with a single Dirac cone edge state, providing a viable candidate for reaching the long-sought topological transport regime. The TlBi film also maintains its nontrivial band topology for a range of hydrogen coverages, indicating that the QSH phase in this film is likely to be particularly robust against bonding effects of substrates. Our predicted QSH buckled honeycombs could be grown or sandwiched between appropriate nanostructures for potential device applications.

■ ASSOCIATED CONTENT

Supporting Information

The Supporting Information is available free of charge on the ACS Publications website at DOI: 10.1021/acs.nanolett.5b02293.

A brief description of the methods and structures, along with detailed tables giving the lattice parameters, energy gaps, and Z_2 invariants of the investigated films (PDF)

■ AUTHOR INFORMATION

Corresponding Authors

*E-mail: fchuang@mail.nsysu.edu.tw.
*E-mail: nilnish@gmail.com.

Notes

The authors declare no competing financial interest.

■ ACKNOWLEDGMENTS

FCC acknowledges support from the National Center for Theoretical Sciences and the Taiwan Ministry of Science and Technology under Grants Nos. MOST-101-2112-M-110-002-MY3 and MOST-101-2218-E-110-003-MY3. He is also grateful to the National Center for High-performance Computing for computer time and facilities. The work at Northeastern University was supported by the US Department of Energy (DOE), Office of Science, Basic Energy Sciences grant number DE-FG02-07ER46352 (core research), and benefited from Northeastern University's Advanced Scientific Computation Center (ASCC), the NERSC supercomputing center through DOE grant number DE-AC02-05CH11231, and support (applications to layered materials) from the DOE EFRC: Center for the Computational Design of Functional Layered Materials (CCDM) under DE-SC0012575. H.L. acknowledge the Singapore National Research Foundation for support under NRF Award No. NRF-NRFF2013-03.

■ REFERENCES

(1) Kane, C. L.; Mele, E. J. *Phys. Rev. Lett.* **2005**, *95*, 146802.
(2) Hasan, M. Z.; Kane, C. L. *Rev. Mod. Phys.* **2010**, *82*, 3045.
(3) Bernevig, B. A.; Hughes, T. L.; Zhang, S.-C. *Science* **2006**, *314*, 1757.
(4) König, M.; Wiedmann, S.; Brüne, C.; Roth, A.; Buhmann, H.; Molenkamp, L. W.; Qi, X.-L.; Zhang, S.-C. *Science* **2007**, *318*, 766.
(5) Roth, A.; Brüne, C.; Buhmann, H.; Molenkamp, L. W.; Maciejko, J.; Qi, X.-L.; Zhang, S.-C. *Science* **2009**, *325*, 294.
(6) Liu, C.; Hughes, T. L.; Qi, X.-L.; Wang, K.; Zhang, S.-C. *Phys. Rev. Lett.* **2008**, *100*, 236601.
(7) Knez, I.; Du, R.-R.; Sullivan, G. *Phys. Rev. Lett.* **2011**, *107*, 136603.
(8) Castro Neto, A. H.; Guinea, F.; Peres, N. M. R.; Novoselov, K. S.; Geim, A. K. *Rev. Mod. Phys.* **2009**, *81*, 109.
(9) Liu, C. C.; Feng, W. X.; Yao, Y. *Phys. Rev. Lett.* **2011**, *107*, 076802.
(10) Tsai, W.-F.; Huang, C.-Y.; Chang, T.-R.; Lin, H.; Jeng, H.-T.; Bansil, A. *Nat. Commun.* **2013**, *4*, 1500.

DOI: 10.1021/acs.nanolett.5b02293
Nano Lett. XXXX, XXX, XXX−XXX

(11) Liu, C. C.; Jiang, H.; Yao, Y. *Phys. Rev. B: Condens. Matter Mater. Phys.* **2011**, *84*, 195430.
(12) Wada, M.; Murakami, S.; Freimuth, F.; Bihlmayer, G. *Phys. Rev. B: Condens. Matter Mater. Phys.* **2011**, *83*, 121310.
(13) Huang, Z.-Q.; Chuang, F.-C.; Hsu, C.-H.; Liu, Y.-T.; Chang, H.-R.; Lin, H.; Bansil, A. *Phys. Rev. B: Condens. Matter Mater. Phys.* **2013**, *88*, 165301.
(14) Liu, Z.; Liu, C. X.; Wu, Y. S.; Duan, W. H.; Liu, F.; Wu, J. *Phys. Rev. Lett.* **2011**, *107*, 136805.
(15) Huang, Z.-Q.; Hsu, C.-H.; Chuang, F.-C.; Liu, Y.-T.; Lin, H.; Su, W.-S.; Ozolins, V.; Bansil, A. *New J. Phys.* **2014**, *16*, 105018.
(16) Chuang, F.-C.; Hsu, C.-H.; Chen, C.-Y.; Huang, Z.-Q.; Ozolins, V.; Lin, H.; Bansil, A. *Appl. Phys. Lett.* **2013**, *102*, 022424.
(17) Zhang, P.; Liu, Z.; Duan, W.; Liu, F.; Wu, J. *Phys. Rev. B: Condens. Matter Mater. Phys.* **2011**, *85*, 201410.
(18) Sofo, J. O.; Chaudhari, A. S.; Barber, G. D. *Phys. Rev. B: Condens. Matter Mater. Phys.* **2007**, *75*, 153401.
(19) Zhang, C. H.; Yan, S. S. *J. Phys. Chem. C* **2012**, *116*, 4163−4166.
(20) Wang, R.; Wang, S.; Wu, X. *J. Appl. Phys.* **2014**, *116*, 024303.
(21) Xu, Y.; Yan, B.; Zhang, H.-J.; Wang, J.; Xu, G.; Tang, P.; Duan, W.; Zhang, S.-C. *Phys. Rev. Lett.* **2013**, *111*, 136804.
(22) Chou, B.-H.; Huang, Z.-Q.; Hsu, C.-H.; Chuang, F.-C.; Liu, Y.-T.; Lin, H.; Bansil, A. *New J. Phys.* **2014**, *16*, 115008.
(23) Hsu, C.-H.; Huang, Z.-Q.; Chuang, F.-C.; Kuo, C.-C.; Liu, Y.-T.; Lin, H.; Bansil, A. *New J. Phys.* **2015**, *17*, 025005.
(24) Liu, C. C.; Guan, S.; Song, Z.; Yang, S. A.; Yang, J.; Yao, Y. *Phys. Rev. B: Condens. Matter Mater. Phys.* **2014**, *90*, 085431.
(25) Song, Z.; Liu, C. C.; Yang, J.; Han, J.; Ye, M.; Fu, B.; Yang, Y.; Niu, Q.; Lu, J.; Yao, Y. *NPG Asia Mater.* **2014**, *6*, e147.
(26) Elias, D. C.; Nair, R. R.; Mohiuddin, T. M. G.; Morozov, S. V.; Blake, P.; Halsall, M. P.; Ferrari, A. C.; Boukhvalov, D. W.; Katsnelson, M. I.; Geim, A. K. *Science* **2009**, *323*, 610−613.
(27) Garcia, J. C.; de Lima, D. B.; Assali, L. V. C.; Justo, J. F. *J. Phys. Chem. C* **2011**, *115*, 13242−13246.
(28) Zhuang, H. L.; Singh, A. K.; Hennig, R. G. *Phys. Rev. B: Condens. Matter Mater. Phys.* **2013**, *87*, 165415.
(29) Chuang, F.-C.; Yao, L.-Z.; Huang, Z.-Q.; Liu, Y.-T.; Hsu, C.-H.; Das, T.; Lin, H.; Bansil, A. *Nano Lett.* **2014**, *14*, 2505−2508.
(30) Fu, L.; Kane, C. L.; Mele, E. J. *Phys. Rev. Lett.* **2007**, *98*, 106803.
(31) Qi, X.-L.; Hughes, T. L.; Zhang, S.-C. *Phys. Rev. B: Condens. Matter Mater. Phys.* **2008**, *78*, 195424.
(32) Fu, L.; Kane, C. L. *Phys. Rev. Lett.* **2009**, *102*, 216403.
(33) Ferhat, M.; Zaoui, A. *Phys. Rev. B: Condens. Matter Mater. Phys.* **2006**, *73*, 115107.
(34) Keen, B.; Makin, R.; Stampe, P. A.; Kennedy, R. J.; Sallis, S.; Piper, L. J.; McCombe, B.; Durbin, S. M. *J. Electron. Mater.* **2014**, *43*, 914.
(35) Kresse, G.; Hafner, J. *Phys. Rev. B: Condens. Matter Mater. Phys.* **1993**, *47*, 558;Kresse, G.; Furthmuller, J. *Phys. Rev. B: Condens. Matter Mater. Phys.* **1996**, *54*, 11169.
(36) Fukui, T.; Hatsugai, Y. J. *J. Phys. Soc. Jpn.* **2007**, *76*, 053702.
(37) Huang, Z.-Q.; Chou, B.-H.; Hsu, C.-H.; Chuang, F.-C.; Lin, H.; Bansil, A. *Phys. Rev. B: Condens. Matter Mater. Phys.* **2014**, *90*, 245433.
(38) Fu, L.; Kane, C. L. *Phys. Rev. B: Condens. Matter Mater. Phys.* **2007**, *76*, 045302.
(39) Chuang, F.-C.; Huang, Z.-Q.; Lin, W.-H.; Albao, M. A.; Su, W.-S. *Nanotechnology* **2011**, *22*, 135703.
(40) Krukau, A. V.; Vydrov, O. A.; Izmaylov, A. F.; Scuseria, G. E. *J. Chem. Phys.* **2006**, *125*, 224106.

DOI: 10.1021/acs.nanolett.5b02293
Nano Lett. XXXX, XXX, XXX−XXX